Rb intercalation of $1T$-$TaSe_2$ studied by photoelectron spectroscopy

S. E. Stoltz and H. I. Starnberg*
Department of Physics, Göteborg University and Chalmers University of Technology, SE-412 96 Göteborg, Sweden

L. J. Holleboom
Department of Computer Science, Karlstad University, SE-651 88 Karlstad, Sweden
(Received 8 October 2002; published 14 March 2003)

The electronic structure of the layered compound $1T$-$TaSe_2$, before and after deposition of Rb, was studied by angle-resolved photoelectron spectroscopy. Core level spectra verified that the deposited Rb intercalated, with only small amounts remaining on the surface. Valence band spectra revealed major changes in the electronic structure, but good agreement with calculations was found for the bands of Se $4p$ character. In contrast, the Ta $5d$ bands were modified by the presence of a strong charge density wave, which was significantly affected by the Rb intercalation. The intercalation also caused a metal to semiconductor transition, although possibly not completely. The observed changes can be attributed to charge transfer, weakened coupling between the layers and reduced hybridization between Se $4p$ and Ta $5d$ states. Comparisons are made with related systems.

DOI: 10.1103/PhysRevB.67.125107 PACS number(s): 79.60.Bm, 71.20.Tx

I. INTRODUCTION

Intercalation compounds formed by insertion of foreign atoms or molecules in layered transition metal dichalcogenides (TMDC's) have been studied extensively during the recent decades.[1–4] These efforts have been motivated both by the suitability of these materials as model systems for a wide range of interesting phenomena and by their potential for practical applications, e.g., in battery technology.

The formula unit for the TMDC's is TX_2, where T is a transition metal (e.g., Ta) and X stands for S, Se, or Te. Each layer consists of a hexagonal sheet of transition metal atoms, sandwiched between two hexagonal chalcogen sheets. In the $1T$ polytype, the coordination of the transition metal by the chalcogen atoms is octahedral, as shown in Fig. 1. The internal bonds in the layers are strong and of mixed ionic and covalent character, while the bonds between adjacent layers are weak and mainly of van der Waals character. Due to this highly anisotropic bonding, one may obtain clean surfaces of high quality by cleavage *in vacuo*, which is a significant experimental advantage. It is the weakness of the interlayer bonds which opens the possibility to intercalate, e.g., alkali metals between the layers, as the energy needed to make room for alkali ions between the layers is relatively small. The electronic structure will change upon alkali metal intercalation, both because of the filling of the valence band and because of the decoupling of the layers as their separation increases.[4,5]

Intercalation with small alkali atoms like Na or Li is suitable in studies of the valence band filling, but if one particularly wants to study the effect of increased layer separation, intercalation with Cs is the most interesting. Intercalation with the intermediately sized alkali metals K and Rb is less studied.

Recently it was reported that Rb deposited *in situ* on various TMDC crystals formed nanowire networks with mesh sizes of ~ 1 μm, preferably along small irregularities on the extremely flat TMDC surfaces.[6] This effect was studied for a number of different TMDC's, both metallic ($1T$-TaS_2, $TiTe_2$, VSe_2) and semiconducting (WSe_2, HfS_2, TiS_2). In subsequent detailed studies of Rb adsorption on $1T$-TaS_2 (Refs. 7 and 8) and $TiTe_2$ (Ref. 9) it was concluded that the observed changes in the electronic structure were induced by the nanowire formation, rather than by intercalation. This is in strong contrast to earlier studies of alkali metal deposition on TMDC surfaces.

The present study is done on $1T$-$TaSe_2$, which is very similar to $1T$-TaS_2. Our aim has been to clarify how Rb behaves when deposited on surfaces of these and other TMDCs, and how the electronic structure of the host materials is modified. Both $1T$-$TaSe_2$ and $1T$-TaS_2 have strong charge density waves (CDW's) at room temperature, and it is known that alkali metal deposition on these materials modifies the CDW's significantly.[7,8,10–12] Any new results which contribute to the understanding of these changes should be of particular interest.

II. EXPERIMENTAL DETAILS

Core level and valence band spectra from $1T$-$TaSe_2$, both before and after Rb deposition, were measured at beamline 33 of the MAX-lab synchrotron radiation facility in Lund, Sweden. This beamline includes a spherical grating monochromator providing photons with energies in the range 15–200 eV and an endstation with a Vacuum Generators ARUPS 10 angle-resolving electron energy analyzer. The synchrotron radiation was incident at an angle of 45° and polarized in the plane of incidence. The overall energy resolution was typically ~ 0.1 eV. The pressure in the UHV system was in the 10^{-10} mbar range or lower in both spectrometer and preparation chambers during the measurements, which were all performed in a single experimental run.

The $1T$-$TaSe_2$ single crystal was attached to the sample holder by silver filled epoxy resin, and a clean mirrorlike (0001) surface was obtained by cleavage *in vacuo*.

The sample was azimuthally oriented by low-energy elec-

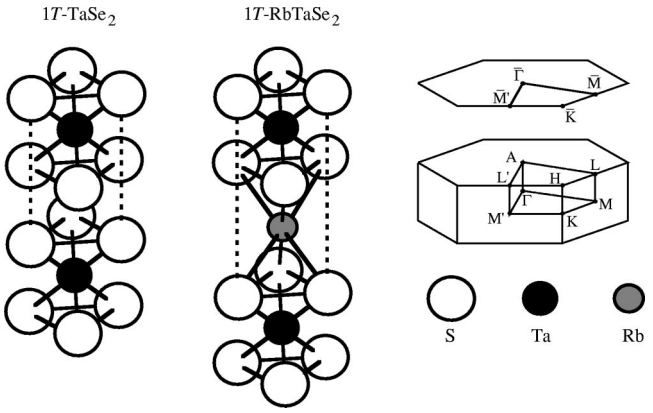

FIG. 1. The crystallographic structures of $1T$-$TaSe_2$ and hypothetical $1T$-$RbTaSe_2$. The corresponding surface and bulk Brillouin zones are shown to the left.

tron diffraction (LEED) for measurements along the $\overline{\Gamma K M}$ and $\overline{\Gamma M}$ directions, respectively. The position of the Fermi level was determined by measurement from a Ta foil in electrical contact with the sample. All binding energies (BE's) are given relative to the Fermi level.

After measuring reference core level and valence band spectra from the host crystal, Rb was deposited *in situ* from a carefully outgassed SAES getter source. The Rb source was operated at a current of 6.0 A for 5 min, which should correspond to a Rb coverage on the sample surface of several monolayers. During the Rb deposition, the pressure in the preparation chamber increased from 5×10^{-11} mbar to 8×10^{-10} mbar.

III. EXPERIMENTAL RESULTS

A. Core levels

The Ta $4f$ spectra before and after the Rb deposition are shown in Fig. 2(a). The deposition increased the CDW splitting of the spin-orbit doublet by shifting the high-BE peaks downwards, while the position of the low-BE components were not effected. Also, the intensity of all peaks increased.

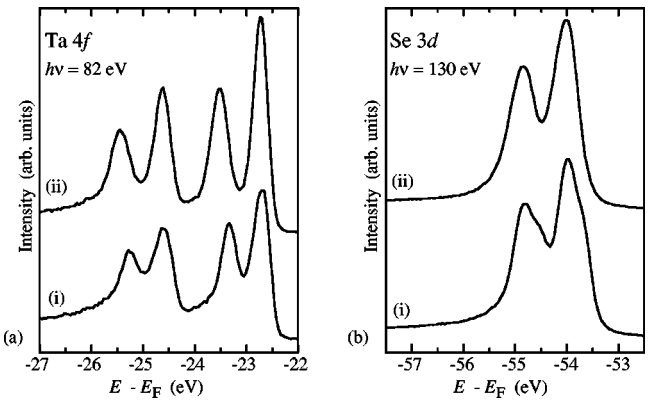

FIG. 2. (a) Ta $4f$ core level spectra obtained before (i) and after (ii) Rb deposition. (b) The corresponding Se $3d$ core level spectra. In both panels the spectra are normalized to have the same background intensity.

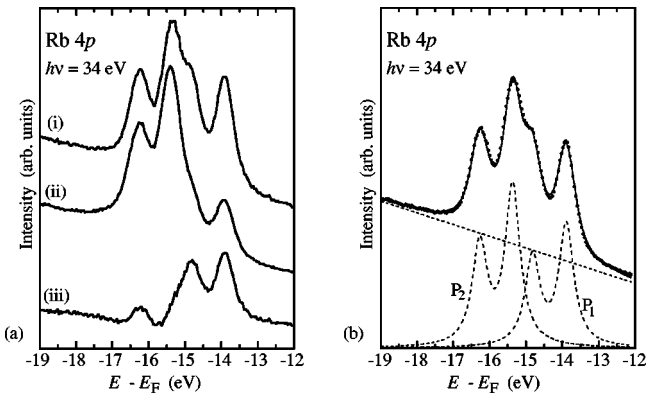

FIG. 3. (a) Rb $4p$ core level spectra obtained after Rb deposition onto $1T$-$TaSe_2$. The spectra (i) and (ii) were obtained at polar emission angles $\theta=0°$ and 75°, respectively, while (iii) is the difference spectrum. (b) The data points (dots) of spectrum (i) together with a fitted curve (solid line), composed of a linear background and the two doublet peaks P_1 and P_2 (dashed lines). Details of the fitting procedure are given in the text.

The Se $3d$ spectra before and after the Rb deposition are shown in Fig. 2(b). Before the deposition a shoulder was visible for each peak on the low-BE side, ~0.3 eV from the main peaks. After the Rb deposition the shoulder was absent, and the spin-orbit doublet was slightly shifted (~0.05 eV) towards higher BE.

The Rb $4p$ spectra after the Rb deposition are shown in Fig. 3(a). They were measured both at normal emission and at polar emission angle $\theta=75°$. The most striking difference between the two spectra is the large difference in the intensity of the lowest-BE peak and the disappearence of the shoulder on the low-BE side of the middle peak.

Ta $4f$, Se $3d$, and Rb $4p$ spectra were also recorded after an additional 2×5 min Rb deposition at 6 A (in total 3×5 min at 6 A), but did not show any significant changes, compared to the spectra obtained after the first Rb deposition.

B. Valence bands

Valence band spectra were measured with $h\nu=24$ eV, both before and after the Rb deposition. The spectra were measured along the $\overline{\Gamma K M}$ azimuthal direction with θ in the range $-30°$ to 75°. Negative polar angles denotes emission directions on the same side of the surface normal as the incident light beam.

The full angular series of valence band spectra are not shown here, but the results are instead presented as structure plots in Sec. IV D. The normal emission spectra before and after Rb deposition are shown in Fig. 4. Figure 5 shows the uppermost parts of the spectra with θ in the range $-15°$ to 15° both before and after the Rb deposition. Both these figures illustrate the significant changes caused by the deposition.

IV. DISCUSSION

A. Rb intercalation

There are four clearly visible components in the normal emission Rb $4p$ spectrum (i) in Fig. 3(a). Spectrum (ii), ob-

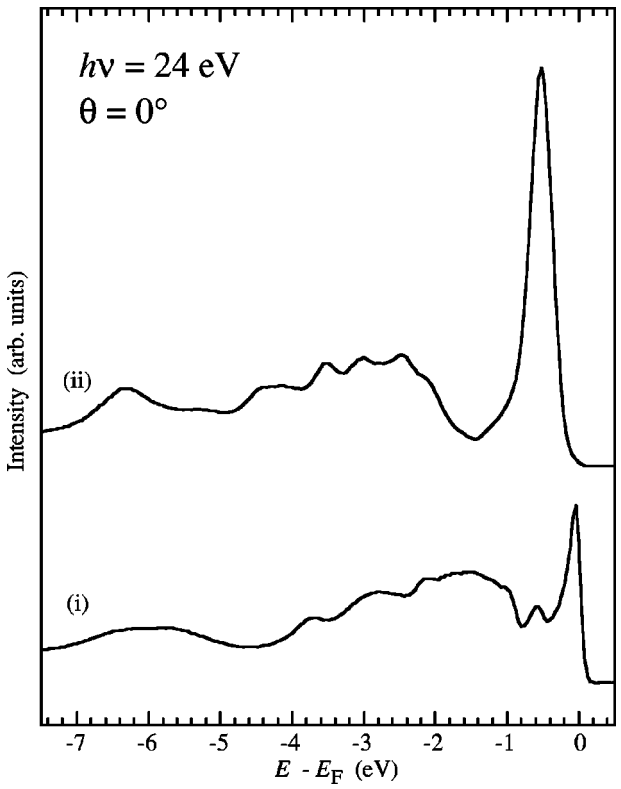

FIG. 4. Normal emission valence band spectra measured before (i) and after (ii) Rb deposition.

tained with the polar emission angle $\theta = 75°$, shows a drastically reduced intensity of the two features of lowest BE. The difference spectrum (iii) confirms that the main effect of the increased emission angle is an intensity loss in a peak doublet with ~ 1.5 eV lower BE than the less affected remaining doublet, although a slight difference in peak widths prevents a complete elimination of the latter doublet in spectrum (iii). Our interpretation is that the measured Rb $4p$ spectra are superpositions of two spin-orbit split doublets: one corresponding to Rb adsorbed on the surface and the other corresponding to intercalated Rb. The intensity decrease of the latter component at large emission angles is then a straightforward consequece of the small photoelectron escape length.

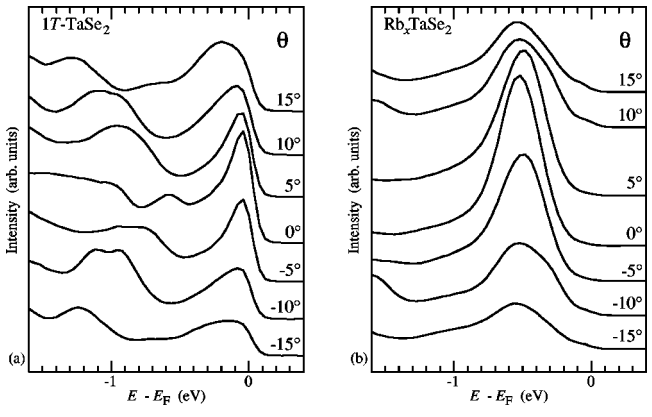

FIG. 5. The upper parts of valence band spectra obtained (a) before and (b) after Rb deposition. The spectra were measured at polar emission angles θ ranging from $-15°$ to $15°$ in the $\overline{\Gamma K M}$ azimuthal direction. The emission angle was counted negative when the emission direction was on the same side of the surface normal as the light beam, positive when on the other side. The photon energy was 24 eV.

To obtain a more accurate analysis of the Rb $4p$ emission, we have applied a numerical peak-fitting procedure to spectrum (i) in Fig. 3(a). The result of this fitting procedure is presented in Fig. 3(b), which shows the measured spectrum (dots) compared with a fitted curved (solid line), which was obtained from a superposition of two spin-orbit split doublets (P_1 and P_2) and a linear background, convoluted with a Gaussian. The equation for the fitted curve is

$$S(E) = \int [P_1(E') + P_2(E') + B(E')] G(E - E') dE', \tag{1}$$

where $G(E-E')$ is a Gaussian with unit area (standard deviation σ). The spin-orbit split doublets are given by

$$P_1(E) = i_1 \{ L_1(E - E_{peak_1}) + r_1 L_2[E - (E_{peak_1} - E_{so_1})] \}, \tag{2}$$

$$P_2(E) = i_2 \{ L_1(E - E_{peak_2}) + r_2 L_2[E - (E_{peak_2} - E_{so_2})] \}, \tag{3}$$

and the linear background is given by $B(E) = k_1 E + k_0$. In Eqs. (2) and (3), i_1 and i_2 denote the intensities of the low-BE components of the spin-orbit doublets, r_1 and r_2 denote the branching ratios between the $p_{1/2}$ and the $p_{3/2}$ components, and E_{peak_1} and E_{peak_2} denote the BE's of the low-BE components of each doublet, while E_{so_1} and E_{so_2} denote the energy splittings. L_1 and L_2 are Lorentzian functions of widths α_1 and α_2 given by

$$L_i(E) = \frac{1}{1 + \alpha_i E^2}. \tag{4}$$

The full width at half maximum (FWHM) equals $2/\sqrt{\alpha_i}$.

The fitted curve in Fig. 3(b) was obtained by using the following values: $i_1 = 50100$, $i_2 = 38000$, $r_1 = 0.637$, $r_2 = 0.735$, $E_{peak1} = -15.37$ eV, $E_{peak_2} = -13.89$ eV, $E_{so_1} = 0.90$ eV, $E_{so_2} = 0.93$ eV, $\alpha_1 = 16.2$ eV^{-2}, $\alpha_2 = 16.4$ eV^{-2}, $\sigma = 0.1$ eV, $k_1 = -3680$ eV^{-1}, and $k_0 = -23800$.

The model used is highly simplified: the line shape asymmetry caused by metallic screening and CDW-induced effects have both been neglected, and the use of a linear background is also a coarse approximation. Therefore it is not surprising that the branching ratios deviate from the theoretically expected values. The spin-orbit splitting of P_1 found is less accurate as the high-BE component appears only as a shoulder in the measured spectrum. The fit should still yield the BE's of the other peaks with high accuracy. The intensity ratio between P_1 and P_2 should also be reasonably accurate, although the use of a linear background may overestimate the P_2 intensity somewhat.

The fitting procedure thus confirms that the measured Rb $4p$ spectra are superpositions of two peak doublets P_1 and P_2 shifted by ~ 1.48 eV with respect to each other. P_2 remains intense at all emission angles, while the intensity of P_1 falls rapidly as the emission angle is increased. The behavior of P_2 is exactly what one would expect from Rb species on top of the surface, while the angular sensitivity of P_1 is difficult to reconcile with anything else than subsurface Rb species. The observed intensity changes in the the two Rb $4p$ pairs is therefore strong evidence that intercalation with Rb has occurred. The BE difference between the two components is furthermore very similar to the BE differences found in other alkali-TMDC systems upon intercalation.[11,13–17] Since photoelectrons from intercalated Rb have to penetrate through at least one full host layer, it is obvious that the corresponding peaks should be strongly damped even at normal emission. That the surface and intercalation related features in Fig. 3 are of similar intensity therefore implies that most of the deposited Rb has indeed intercalated.

Our present results are seemingly in conflict with the findings reported by Adelung *et al.*,[6–9] as they generally observed formation of Rb nanonetworks on TMDC surfaces instead of intercalation. In their detailed study of the Rb/1T-TaS_2 system,[8] they propose that the nanowires form in cracks of the first host layer and that these cracks propagate further by the induced stress. As the fresh cracks are filled by Rb atoms diffusing on the surface, the wires thus grow in a self-sustaining manner. According to this model, the penetrating Rb wires cause the first layer to corrugate and become separated from the next layer, with no intercalated Rb atoms away from the wires. They also attribute the occurrence of different CDW superstructures to whether the Rb wire networks are open or closed.

The STM results by Adelung *et al.* firmly prove that Rb deposition on TMDC surfaces results in formation of metallic wire networks under certain conditions. Since we have not used STM in our present study, we cannot exclude the presence of metallic Rb wires on our sample surface, but our Rb $4p$ spectra nevertheless provide strong evidence that, under our deposition conditions, most of the Rb does intercalate.

If Rb deposition may lead to either wire formation or intercalation, it is of great interest to sort out which conditions favors which outcome. A reported requirement for wire formation is that the Rb source should be operated at high temperature.[6,8] It was proposed that the adsorbed Rb atoms would otherwise not attain high enough kinetic energies for diffusion to the ''folds'' or cracks were the wires formed. Also the higher Rb flux obtained with a hotter source might be of crucial importance for the outcome. If metallic islands or wires are more stable against intercalation than dispersed alkali metal atoms, as hinted by a low-temperature study of the Cs/TiS_2 system,[18] and if there is a competition between intercalation and wire formation, it seems reasonable that higher flux should favor wire formation through an increased probability for adsorbed atoms to interact with each other before there is a possibility of intercalation. The behavior of Rb atoms adsorbed on TMDC surfaces may also be profoundly influenced by the presence of contaminants. Alkali-intercalated TMDC samples can be de-intercalated by exposure to oxidizing species,[19,20] and if, e.g., oxygen is present on the surface during the deposition, it may have a significant effect on the adsorbtion and perhaps inhibit the intercalation completely. The valence band spectra measured from different Rb/1T-TaS_2 systems by Adelung *et al.*[8] are dominated by broad features around 5–6 eV BE, which are not seen at all in our corresponding spectra from Rb/1T-$TaSe_2$, e.g., spectrum (ii) in Fig. 4. As such broad and intense features are typical for severely contaminated samples, one may suspect that the Rb networks were partially oxidized. If the oxidation occurs already under the deposition, which, e.g., may happen if the source is not sufficiently outgassed before operation, it may have a stabilizing effect on the wires and possibly also inhibit the intercalation.

In the attempts to reconcile our present results from Rb/1T-$TaSe_2$ with those of Adelung *et al.*[8] from the Rb/1T-TaS_2 system, one may also consider the possibility that the latter samples actually were intercalated in addition to the formation of Rb wires. An indication for this is that the valence band spectra show the same type of changes as commonly associated with intercalation. Furthermore, for the related nanowire Rb/$TiTe_2$ system, STM height profiles shows an increased separation (~ 1 Å) between the first two layers.[9] Such an elevation of the first layer across the whole mesh area is hardly possible without any intercalated atoms in the interlayer gap.

In this context it is interesting to compare with the Cs/TiS_2 system, for which a transmission electron microscopy study[20] revealed a network of cracks very similar in appearance to the Rb wire networks. Whether the cracks contained metallic Cs was not examined, but strong evidence for Cs intercalation was found. This example shows that the formation of crack networks on the surface is by no means incompatible with intercalation, but rather should favor it.

B. CDW effects

The charge transfer due to intercalation with Rb changes the shape of the Fermi surface, which is of critical importance to the CDW periodicity. As seen in Fig. 2(a), intercalation with Rb increased the Ta $4f$ CDW splitting from 0.64 eV to 0.80 eV. This effect is the same as found upon intercalation with Cs (Ref. 11) and is qualitatively explained by the model of Crawack and Pettenkofer,[12] by considering the differences in charge distribution between the $\sqrt{13}\times\sqrt{13}$ and c$(2\sqrt{3}\times 4)$ CDW phases.

As the CDW is largely confined to the Ta sheets, it will affect the Se core levels much less than the Ta levels. Consequently the Se $3d$ spectra in Fig. 2(b) mainly show spin-orbit splitting. Only spectrum (i), measured before the intercalation, shows weak shoulders which can be attributed to the influence of the CDW. It is notable that the shoulders are no longer visible in spectrum (ii) obtained after the Rb intercalation. Apparently the CDW becomes even more confined to the Ta sheets after the intercalation. As discussed in Sec. IV E below, this could be due to reduced p-d hybridization in the valence band. Alternative explanations of the shoulders could involve BE differences between bulk and surface

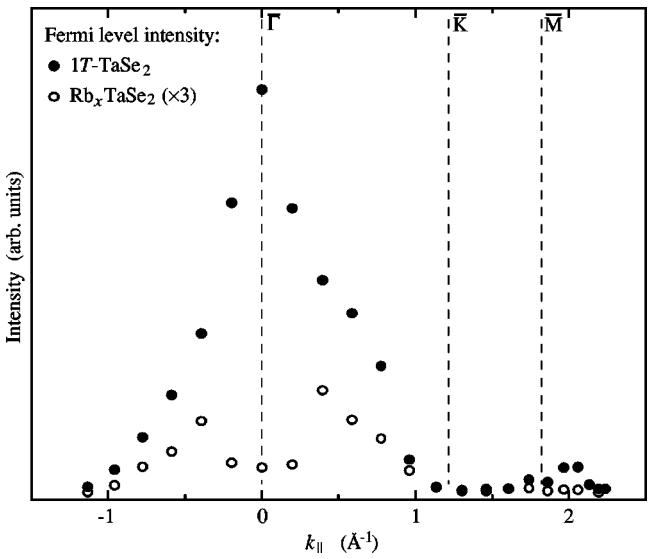

FIG. 6. Photoemission intensity at the Fermi level plotted against $k_\parallel$ in the $\bar{\Gamma}\bar{K}\bar{M}$ azimuthal direction. The photon energy was 24 eV. Prior to evaluation, the spectra were normalized to have equal background intensity. Solid and open circles denote intensities before and after Rb deposition, respectively.

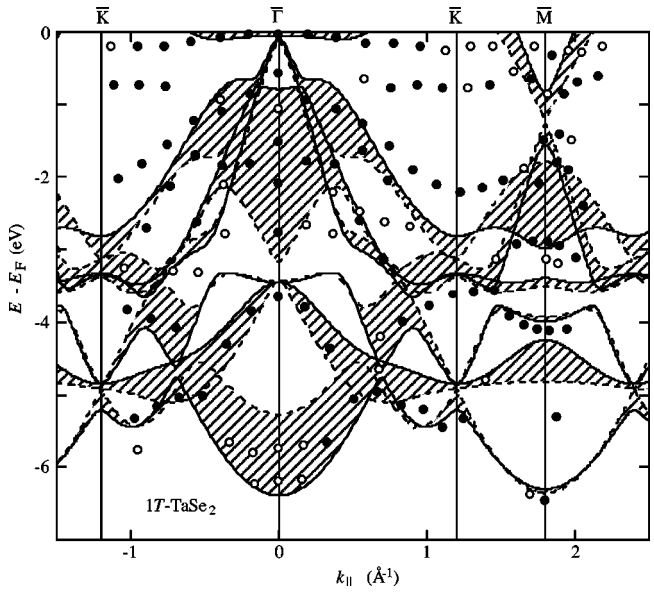

FIG. 7. Structure plot for clean 1T-$TaSe_2$ along the $\bar{\Gamma}\bar{K}\bar{M}$ azimuthal direction. Solid circles correspond to conspicuous spectral peaks, open circles to weaker structures. Comparisons are made with ΓKM (solid lines) and AHL (dashed lines) bands calculated by the LAPW method. The crosshatched areas approximates the surface projected band structure. The experimental points were obtained from spectra measured with $h\nu = 24$ eV.

layers, but the absence of similar Se 3d shoulders in comparable high-resolution spectra from layered selenides without CDW's (Refs. 15 and 17) speaks against such interpretations.

C. Metal to semiconductor transition

Crawack *et al.*[11] have previously reported that the CDW transition induced by Cs intercalation is accompanied by a metal to semiconductor transition. This appears to be the case also for intercalation with Rb. As seen in Figs. 4 and 5 the dominating Ta 5d peak withdraws from the Fermi level, leaving a band gap of ~ 0.5 eV after the intercalation. In agreement with Crawack *et al.*,[11] we believe this is due to a Mott-Hubbard localization in the Ta 5d band. However, on close inspection of Fig. 5(b) one may discern a low-BE shoulder on the main peak for $\theta = \pm 10°$. For these moderately off-normal emission angles there is also a trace of emission reaching up to the Fermi edge. To obtain a clearer picture of this we have evaluated the emission at the Fermi level ($\pm$ the energy resolution) as a function of θ, both before and after the Rb intercalation. The results are presented in Fig. 6, with the emission angles converted to corresponding values of $k_\parallel$, the wave-vector component parallel to the surface. Before the intercalation the intensity peaks strongly at $\bar{\Gamma}$, falls practically to zero at $\bar{K}$, but reappear weakly around $\bar{M}$. After the intercalation the intensities are drastically reduced (although multiplied by a factor of 3 for clarity in Fig. 6). Somewhat unexpectedly, there still remains some significant Fermi level emission, peaking at ± 0.4 Å^{-1} (corresponding to $\pm 10°$ emission angle). This is not likely due to emission from unintercalated deeper layers, because one would then expect the intensity to peak at $\bar{\Gamma}$. Similar Fermi level emission was also observed for for $\theta = \pm 10°$ in the $\bar{\Gamma}\bar{M}$ azimuthal direction (not shown here). From this observation of spectral weight at the Fermi level in different azimuthal directions, one may speculate that the metal to semiconductor transition is not complete, but that an almost circular Fermi surface of radius ~ 0.4 Å^{-1} around $\bar{\Gamma}$ (if perpendicular dispersion is neglected) may remain after the intercalation. The possible origin of such a Fermi surface is discussed in Sec. IV E below.

D. Valence band dispersions

Figures 7 and 8 show the structure plots for pure and Rb intercalated 1T-$TaSe_2$, respectively. They were obtained from the angular series of valence band spectra and show the energy of spectral features plotted against $k_\parallel$ in the $\bar{\Gamma}\bar{K}\bar{M}$ azimuthal direction.[21] Conspicous peaks are represented by solid circles, while shoulders and other weak structures are denoted by open circles. The structure plots can be directly compared with calculated bands, but complications arise as the perpendicular wave-vector component $k_\perp$ is not conserved in the photoemission process. Ideally, the comparison should be with the surface-projected band structure. Our simplified approach in Figs. 7 and 8 is to include calculated bands for the ΓKM and AHL symmetry lines, with the areas between connected pairs of bands crosshatched. These crosshatched areas are a close approximation to the surface-projected band structure. The calculations were self-consistent and scalar relativistic, but did not include spin-orbit splitting. They were done by the linear augmented plane wave (LAPW) method, and the parametrized Ceperley-Alder[22] form of the exchange-correlation potential was used. The lattice parameters used in the calculations for

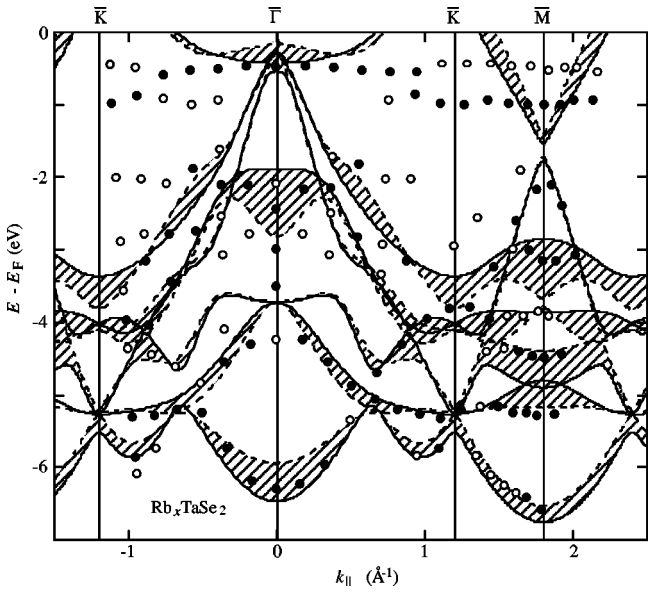

FIG. 8. Same as Fig. 7, but with experimental points obtained after Rb deposition and with calculated bands for the hypothetical $1T$-$RbTaSe_2$ compound.

$1T$-$TaSe_2$ were $a=3.477$ Å and $c=6.272$ Å. For the hypothetical $1T$-$RbTaSe_2$ structure we used $a=3.477$ Å and $c=8.167$ Å.

CDW's can be included in first-principles calculations by the use of supercells, as was recently done by Sharma *et al.*[23] This approach proved valuable for the understanding of CDW stability, but in practice comparison with experimental results is more convenient using non-CDW bands in the unreconstructed Brillouin zone.

The agreement in Fig. 7 between the experimental points and calculated bands is surprisingly good, considering that the CDW superlattice was not included in the calculations. For the Se $4p$ bands the agreement is almost as good as for, e.g., VSe_2, which has the $1T$ structure without any CDW reconstruction at room temperature.[15] The only major deviation is that the uppermost Se $4p$ band around the $\bar{K}$ point appears to have ~ 1 eV lower BE than calculated. The agreement found supports the view that the electronic states predominantly of Se origin are not much affected by the CDW superlattice. In contrast, there are clear CDW effects in the Ta $5d$ bands close to the Fermi energy. Over most of the surface Brillouin zone, two weak nondispersive structures are seen in the range 0–1 eV BE. This is in qualitative agreement with the simple model of Smith *et al.*,[24] according to which the lowest Ta $5d$ band is split up into three subband manifolds by the CDW superlattice potential. The observation of two, rather than three, peaks can be attributed to resolution and photoemission cross-section effects. Around $\bar{\Gamma}$ the Ta $5d$ emission is significantly different, however, with a very intense peak appearing immediately below the Fermi level. This peak gives rise to the strong Fermi level emission also evident in Fig. 6, and it is striking how well the range in **k** space with high intensity corresponds to the range where the calculated Ta $5d$ band straddles the Fermi level. This agreement, which is commensurate with the metallic nature of $1T$-$TaSe_2$,[25] suggests that the effects of the CDW on this portion of the Fermi surface and the states producing it are very limited. This does not exclude Fermi surface nesting as an important condition for the CDW formation, however, as the nesting primarily should involve portions of the Fermi surface around $\bar{M}$. In qualitative agreement with this, there are no visible Fermi level crossings around $\bar{M}$ in Fig. 7.

Figure 8 shows that the agreement between experimental results and calculated bands after intercalaton with Rb is even better than for the pure host material, with exception for the Ta $5d$ bands. This is particularly remarkable as the calculations were done for the fully intercalated $RbTaSe_2$ compound with the hypothetical $1T$ structure shown in Fig. 1. The only adjustment done to the calculated band structure was an upward energy shift by ~ 0.1 eV to compensate for a smaller band filling than in the fully intercalated compound. A major difference from the $1T$-$TaSe_2$ band structure is that the perpendicular dispersion is significantly smaller after the intercalation. Like increased band filling, this seems to be a general effect of alkali metal intercalation in TMDCs.[4] However, for the Ta $5d$ band the agreement is very poor, which can be attributed to a much stronger effect of the CDW superlattice on the Fermi surface than before the intercalation. Two experimental structures without significant dispersion are seen: One peak with 1.0 eV BE dominates over much of the Brillouin zone, but becomes invisible close to $\bar{\Gamma}$. Possibly it is just concealed by overlap with the tail of the other peak, with 0.5 eV BE, which is particularly intense here. The latter peak is seen at all emission angles, but the range in **k** space with high intensity coincides remarkably with the range around $\bar{\Gamma}$ for which the lowest Ta $5d$ band should be occupied in the absence of the CDW, according to the band calculation. Unlike the calculated band it does not disperse toward the Fermi level away from $\bar{\Gamma}$, however. The Fermi level band crossing hinted in Fig. 6 agrees roughly with the calculated crossing in Fig. 8, but is not seen in the structure plot since the corresponding feature is to weak for direct observation as a peak.

The nondispersive Ta $5d$ bands imply that the CDW states are strongly correlated, and it is therefore important that correlation effects are properly accounted for in any calculations aimed at descibing the Ta $5d$ emission.

E. Significance of *p*-*d* hybridization

The comparison between experimental structure plots and calculated bands for $1T$-$TaSe_2$ before and after Rb intercalation indicates that the influence of the CDW's on the Se $4p$ bands is very weak, so that these bands are reasonably well described in terms of the unreconstructed Brillouin zone. This is not unexpected, as the electronic states involved in the CDW are mainly of Ta $5d$ character and largely localized in the Ta atomic layers. As expected the Ta $5d$ emission shows stronger CDW effects, but there is a surpisingly large difference between the results obtained before and after the Rb deposition: After intercalation the Ta $5d$ band is reconstructed into two subbands without significant dispersion and most, if not all, of the Fermi surface apparently is destroyed,

probably through a Mott-Hubbard transition. CDW-induced nondispersive Ta $5d$ subbands were seen also before the intercalation, but only weakly, and the dominating Ta $5d$ peak indicated a Fermi surface around $\bar{\Gamma}$ in fairly good agreement with the calculated non-CDW band structure. Obviously there is less Fermi surface gapping in the pure $1T$-$TaSe_2$ and no sign of any metal to semiconductor transition. It appears very likely that these differences are connected with changes in the p-d hybridization upon intercalation. Of the three upper Se $4p$ bands near the Γ point, two are dominated by p_x and p_y orbitals and have very small perpendicular dispersion, while the third is of p_z character with considerable perpendicular dispersion. From Fig. 7 it is clear that the bands of p_x and p_y character get very close to the Ta $5d$ band at Γ in the pure $1T$-$TaSe_2$, while the top of the p_z band is found $\sim$0.7 eV below. Since the p_z orbitals are directed perpendicular to the layers, this latter band is very likely to hybridize with the Ta $5d$ band. The mixing of Se $4p$ character into the Ta $5d$ states should make the latter less localized and counteract any tendency of Mott-Hubbard localization. The CDW effects should also be reduced in the **k** space region with strong hybridization. The lower reconstructed Ta $5d$ subband seems to be completely removed in this region, where it otherwise would have overlapped with the top of the p_z band. As can be seen in Fig. 8, the bands of p_x and p_y character are relatively unchanged after the intercalation. Because of the orientation and symmetry of these orbitals, the hybridization effects remain small, despite a direct energy overlap with the Ta $5d$ band at Γ. In contrast, the p_z band is strongly affected by the intercalation. As a consequence of the weakened interlayer coupling, the perpendicular dispersion is reduced by a factor of $\sim$0.4, so that the top of the band after intercalation is found almost 2 eV below the Fermi level. The increased separation from the Ta $5d$ band should lead to much weaker hybridization, leaving the Ta $5d$ states more localized with sufficiently strong correlation to drive a metal to semiconductor transition. The CDW should also be stronger, but the apparent weakening of the lower subband emission around Γ may involve some remaining p-d hybridization.

Also the observed changes in the Se $3d$ core level could be associated with changes in p-d hybridization. As pointed out before, the CDW is mainly localized in the Ta atomic layers, why the Ta core levels should be much more affected than the Se core levels by the CDW induced variations in the electrostatic potential. However, the more Se p states that are mixed into the Ta $5d$ bands, the more of the CDW is also transfered to the Se layers. Therefore one may expect the Se core levels to be more affected by the CDW the stronger the hybridization is, unless it is so strong that the CDW is destroyed. On the basis of this, we tentatively attribute the shoulders seen in Se $3d$ spectrum (i) in Fig. 2(b) to CDW splitting. After the intercalation with Rb the p-d hybridization is weaker, and the CDW amplitude in the Se layers is reduced to the extent that the CDW splitting is not resolved in spectrum (ii).

In order to map the Ta $5d$ emission around $\bar{\Gamma}$ in more detail, we have used the spectra in Fig. 5 to construct refined

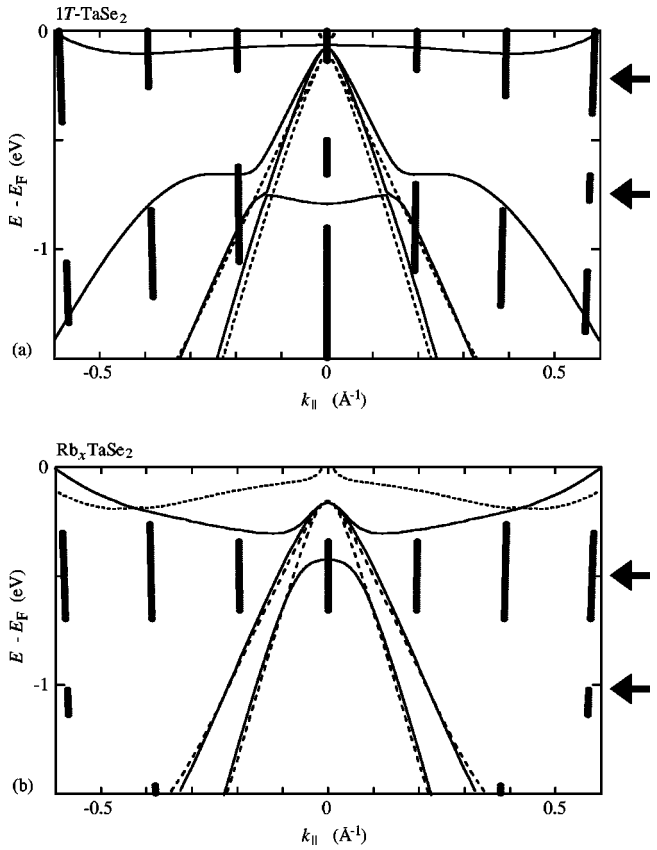

FIG. 9. Refined structure plots for (a) clean $1T$-$TaSe_2$ and (b) after intercalation with Rb. The plots compare the experimental peaks from the spectra in Fig. 5 with the calculated bands near the Fermi level around the $\bar{\Gamma}$ point in the $\bar{\Gamma}\bar{K}\bar{M}$ azimuthal direction. The experimental peaks are represented by vertical bars extending over the energy ranges for which the corresponding spectral curves have negative second derivative. The bars obtained in this way shows both widths and positions of the peaks. Like in Figs. 7 and 8, the calculated bands along ΓKM and AHL are shown as solid and dashed lines, respectively.

structure plots, which are presented in Fig. 9. Instead of marking only the center position, the peaks are here represented by vertical bars, each one extending over the energy range where the second derivative of the corresponding spectral curve is negative. Structure plots generated by this procedure do not depend on any subjective judgement and have the advantage that also the widths of the peaks are represented. The calculated LAPW bands along the ΓKM and AHL directions are also shown in Fig. 9 as solid and dashed lines, respectively. The energy positions of the nondispersive CDW subbands visible away from the near-Γ region are indicated by arrows to the right. Figure 9(a) shows that for pure $1T$-$TaSe_2$ there is one peak of clear Ta $5d$ character around Γ which reaches up to the Fermi level. It is particularly narrow at Γ, but away from this point it becomes gradually broader and weaker, and its center position shift slightly downwards, and eventually it merges with the weak upper nondispersive subband visible in other parts of the Brillouin zone. Essentially the same behavior of this peak was observed previously by Horiba *et al.* using a photon en-

ergy of 21.2 eV.[26] About 1 eV below the Fermi level a peak is seen to disperse in qualitative agreement with the Se $4p_z$ band, although the calculated band disperses more rapidly. At Γ it is split up into one narrow peak above the calculated maximum of the p_z band and one broad peak extending downwards. This splitting, which is not reproduced by the LAPW calculation, may involve the combined effects of *p-d* hybridization and the CDW superlattice potential. Figure 9(b) shows the corresponding feature after intercalation with Rb. The intense Ta $5d$ peak is now separated from the Fermi level and coincides with the upper CDW subband. The p_z band is shifted down, and in agreement with this all visible Se $4p$ emission, except a small hint at the very bottom, is found below the energy range shown in the figure. The vanishing of the lower CDW subband emission around Γ may be due to remaining *p-d* hybridization or it is just concealed by overlap with the tail of the upper peak which is very intense here. For $k_{\|}=\pm 0.4$ Å^{-1} the upper Ta $5d$ peak is seen to broaden. This broadening coincides with the maximum in the Fermi level intensity (see Fig. 6) and may indicate overlap with a dispersing feature too weak to be separately resolved. Thus one may speculate that the Mott-Hubbard transition is not complete, but that some dispersive band remains to cross the Fermi level, making the compound a poor metal. Such a dispersive band may have a mixed *p-d* character, and if the character is largely p_x and p_y, that could explain why it is not direcly observed, as the other bands of this character are also invisible at the photon energy used. In this context it may be appropriate to compare with the related compound $1T$-VSe_2, where *p-d* hybridization modified the Fermi surface and was revealed mainly through notable variations in emission intensity from the V $3d$ band.[27]

F. Comparison with the Cs/1*T*-$TaSe_2$ system

The study of the Cs/$1T$-$TaSe_2$ system by Crawack *et al.*[11] did not include detailed valence band mapping, but produced otherwise results almost identical to what we found for the Rb/$1T$-$TaSe_2$ system. Their assignment of surface and intercalation components in Cs core level spectra is completely analogous to our interpretation of Rb $4p$ spectra. They found Cs intercalation to have the same effect on the Ta $4f$ CDW splitting as we obtained with Rb, and also the changes in the Ta $5d$ band seems to be very similar. Since they did not measure angular series of valence band spectra, they did not see evidence for any remaining weak metallicity after Cs intercalation, but that is quite possibly a feature also of the Cs/$1T$-$TaSe_2$ system. Crawack *et al.*[11] used LEED to determine that the CDW periodicity changed from $\sqrt{13}\times\sqrt{13}$ to $c(2\sqrt{3}\times 4)$ upon Cs intercalation. Since there is a strong correlation between Ta $4f$ splitting and CDW periodicity, it seems reasonable to believe that accurate LEED studies of the Rb/$1T$-$TaSe_2$ system would have revealed the same periodicities.

G. Comparison with 1*T*-TaS_2

The closely related compound $1T$-TaS_2 differs from $1T$-$TaSe_2$ by having a more complicated CDW phase diagram. In the low-temperature limit both compounds display the same $\sqrt{13}\times\sqrt{13}$ periodicity, but while $1T$-TaS_2 undergoes a metal to semiconductor transition, $1T$-$TaSe_2$ remains metallic. Calculated band structures (without inclusion of CDW effects) are very similar, but the separation between the Ta $5d$ and S $3p$ bands in $1T$-TaS_2 is significantly larger than beween the corresponding Ta $5d$ and Se $4p$ bands in $1T$-$TaSe_2$.[28,29] This should lead to significantly smaller *p-d* hybridization in $1T$-TaS_2 which, according to the same reasoning as for the Rb-intercalated $1T$-$TaSe_2$, should lead to more localized Ta $5d$ states with stronger correlation effects. We therefore believe that the differences between $1T$-TaS_2 and $1T$-$TaSe_2$ largely are a matter of differences in the *p-d* hybridization. Since much of the *p-d* hybridization in $1T$-$TaSe_2$ is removed by the intercalation, one may expect the alkali metal intercalation compounds of $1T$-TaS_2 and $1T$-$TaSe_2$ to be more similar to each other than the host materials are.

Zwick *et al.*[30] have published a high-resolution photoemission study of the CDW state in $1T$-TaS_2. They found that the splitting of Ta $5d$ states into subbands was clearly associated with the metal to semiconductor transition. In our case the situation is similar, but the transition is forced by intercalation rather than by change of temperature.

V. CONCLUSIONS

Angle-resolved photoelectron spectroscopy has been used to study the electronic structure of $1T$-$TaSe_2$ before and after *in situ* intercalation with Rb. Rb $4p$ core level spectra provides strong evidence that most of the deposited Rb intercalated. Formation of Rb networks instead of intercalation has recently been reported, but we believe that such results require higher deposition rates and/or the presence of oxidizing species.

For the pure $1T$-$TaSe_2$, the valence bands are in fairly good agreement with with calculated non-CDW LAPW bands. The only clear CDW effect is a splitting of the Ta $5d$ band into nondispersive subbands, but around $\bar{\Gamma}$ a Fermi surface is found in agreement with the LAPW calculations. The survival of this Fermi surface can be attributed to strong *p-d* hybridization, which counteracts the Ta $5d$ correlation effects.

The intercalation with Rb gives rise to prominent changes in the electronic band structure by adding more electrons to the host layers and by reducing the surface-perpendicular band dispersion through weakening of the interlayer electronic coupling. The charge transfer alters the CDW periodicity by changing the Fermi surface nesting, and the reduced surface-perpendicular dispersion decreases the hybridization between Se $4p$ and Ta $5d$ states. The Fermi surface around $\bar{\Gamma}$ is destroyed by a Mott-Hubbard transition, but some remaining weak Fermi level spectral weight ~ 0.4 Å^{-1} away from $\bar{\Gamma}$ suggests that the metal to semiconductor transition is not complete. One may speculate that a small circular Fermi surface, involving hybridization with p_x and p_y states, remains around $\bar{\Gamma}$. In contrast, the valence bands of Se $4p$ origin are found to agree very well with the non-CDW LAPW bands.

The Rb intercalation increased the CDW splitting of the Ta $4f$ core level. This change can be explained as consequence of altered CDW periodicity. In contrast, a small CDW splitting of the Se $3d$ core level vanished upon Rb intercalation. This is tentatively an effect of the CDW becoming more confined to the Ta layers through reduced p-d hybridization.

Pure $1T$-$TaSe_2$ has a simpler CDW phase diagram than $1T$-TaS_2 and remains metallic down to zero temperature. We believe that a fundamental reason for this is the stronger p-d hybridization, which weakens the correlation effects in the Ta $5d$ bands.

Clearly, there is a need for continued theoretical and experimental efforts to understand the formation and modification of CDW's in $1T$-TaS_2 and $1T$-$TaSe_2$. Particular attention should be paid to the correlation effects, which are strong in these systems.

ACKNOWLEDGMENTS

We want to thank F. Lévy for providing the $1T$-$TaSe_2$ samples and the staff at MAX-lab for valuable assistance. This work was supported by the Swedish Research Council.

*Electronic address: starn@fy.chalmers.se

[1] *Intercalated Layered Materials*, edited by F. A. Lévy (Reidel, Dordrecht, 1979).
[2] W. Y. Liang, in *Intercalation in Layered Materials*, edited by M. S. Dresselhaus (Plenum, New York, 1979), p. 31.
[3] R. H. Friend and A. D. Yoffe, Adv. Phys. **36**, 1 (1987).
[4] H. I. Starnberg, H. E. Brauer, and H. P. Hughes, in *Electron Spectroscopies Applied to Low-Dimensional Materials*, edited by H. P. Hughes and H. I. Starnberg (Kluwer, Dordrecht, 2000), p. 41.
[5] H. I. Starnberg, H. E. Brauer, L. J. Holleboom, and H. P. Hughes, Phys. Rev. Lett. **70**, 3111 (1993).
[6] R. Adelung, L. Kipp, J. Brandt, L. Tarcak, M. Traving, and C. Kreis, Appl. Phys. Lett. **74**, 3053 (1999).
[7] R. Adelung, J. Brandt, L. Tarcak, L. Kipp, and M. Skibowski, Appl. Surf. Sci. **162–163**, 666 (2000).
[8] R. Adelung, J. Brandt, L. Kipp, and M. Skibowski, Phys. Rev. B **63**, 165327 (2001).
[9] R. Adelung, J. Brandt, K. Rossnagel, O. Seifarth, L. Kipp, M. Skibowski, C. Ramirez, T. Strasser, and W. Schattke, Phys. Rev. Lett. **86**, 1303 (2000).
[10] C. Pettenkofer and W. Jaegermann, Phys. Rev. B **50**, 8816 (1994).
[11] H. J. Crawack, Y. Tomm, and C. Pettenkofer, Surf. Sci. **465**, 301 (2000).
[12] H. J. Crawack and C. Pettenkofer, Solid State Commun. **118**, 325 (2000).
[13] C. Pettenkofer, W. Jaegermann, A. Schellenberger, E. Holub-Krappe, C. Papageorgopoulos, M. Kamaratos, and A. Papageorgopoulos, Solid State Commun. **84**, 921 (1992).
[14] H. E. Brauer, H. I. Starnberg, L. J. Holleboom, and H. P. Hughes, Surf. Sci. **331–333**, 419 (1995).
[15] H. E. Brauer, H. I. Starnberg, L. J. Holleboom, V. N. Strocov, and H. P. Hughes, Phys. Rev. B **58**, 10 031 (1998).
[16] H. E. Brauer, H. I. Starnberg, L. J. Holleboom, V. N. Strocov, and H. P. Hughes, J. Phys.: Condens. Matter **11**, 8957 (1999).
[17] H. E. Brauer, H. I. Starnberg, L. J. Holleboom, H. P. Hughes, and V. N. Strocov, J. Phys.: Condens. Matter **13**, 9879 (2001).
[18] H. I. Starnberg, H. E. Brauer, and V. N. Strocov, Surf. Sci. **384**, L785 (1997).
[19] S. D. Foulias, D. S. Vlachos, C. A. Papageorgopoulos, R. Yavor, C. Pettenkofer, and W. Jaegermann, Surf. Sci. **352–354**, 463 (1996).
[20] M. Remškar, A. Popović, and H. I. Starnberg, Surf. Sci. **430**, 199 (1999).
[21] H. P. Hughes and W. Y. Liang, J. Phys. C **6**, 1684 (1973).
[22] D. M. Ceperley and B. J. Alder, Phys. Rev. Lett. **45**, 566 (1980).
[23] S. Sharma, L. Nordström, and B. Johansson, Phys. Rev. B **66**, 195101 (2002).
[24] N. V. Smith, S. D. Kevan, and F. DiSalvo, J. Phys. C **18**, 3175 (1985).
[25] F. J. DiSalvo and J. E. Graebner, Solid State Commun. **23**, 825 (1977).
[26] K. Horiba, K. Ono, H. W. Yeom, Y. Aiura, O. Shiino, J. H. Oh, T. Kihara, S. Nakazono, M. Oshima, and A. Kakizaki, Physica B **284–288**, 1665 (2000).
[27] M. T. Johnson, H. I. Starnberg, and H. P. Hughes, J. Phys. C **19**, L451 (1986).
[28] A. M. Woolley and G. Wexler, J. Phys. C **10**, 2601 (1977).
[29] P. Aebi, T. Pillo, H. Berger, and F. Lévy, J. Electron Spectrosc. Relat. Phenom. **117–118**, 433 (2001).
[30] F. Zwick, H. Berger, I. Vobornik, G. Margaritondo, L. Forró, C. Beeli, M. Onellion, G. Panaccione, A. Taleb-Ibrahimi, and M. Grioni, Phys. Rev. Lett. **81**, 1058 (1998).